School of Mathematics, Meteorology
and Physics

University of

Department of Mathematics

Preprint MPS_2009-07

4 August 2009

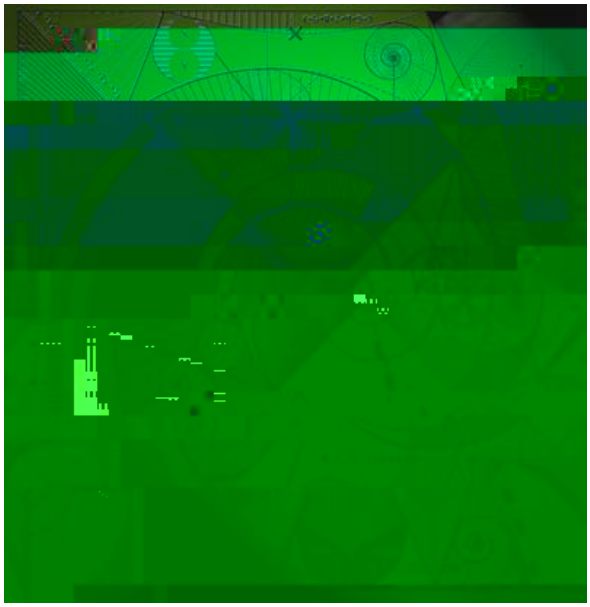

Review

Symmetry-break in Voronoi Tessellations

Valerio Lucarini [1,2,3]

[1] Department of Mathematics, University of Reading, Whiteknights, PO Box 220, Reading RG6 6AX, UK; Email:

Departmem

on framework the properties of the Voronoi tessellations resulting from regular 2D and 3D crystals and those of tessellations generated by Poisson distributions of points, thus analyzing in a common framework symmetry breaking processes and the approach to uniform random distributions of seeds. We perturb crystalline structures in 2D and 3D with a spatial Gaussian noise whose adimensional strength is α and analyze the statistical properties of the cells of the resulting Voronoi tessellations using an ensemble approach. In 2D we consider triangular, square and hexagonal regular lattices, resulting into hexagonal, square and triangular tessellations, respectively. In 3D we consider the simple cubic (SC), body-centered cubic (BCC), and face-centered cubic (FCC) crystals, whose corresponding Voronoi cells are the cube, the truncated octahedron, and the rhombic dodecahedron, respectively. In 2D, for all values $\alpha>0$, hexagons constitute the most common class of cells. Noise destroys the triangular and square tessellations, which are structurally unstable, as their topological properties are discontinuous in $\alpha=0$. On the contrary, the honeycomb hexagonal tessellation is topologically stable and, experimentally, all Voronoi cells are hexagonal for small but finite noise with $\alpha<0.12$. Basically, the same happens in the 3D case, where only the tessellation of the BCC crystal is topologically stable even against noise of small but finite intensity. In both 2D and 3D cases, already for a moderate amount of Gaussian noise ($\alpha>0.5$), memory of the specific initial unperturbed state

tessellation, which in the 2D case is the hexagonal honeycomb one, is obtained. In any case, it is found that the gamma distributions provide excellent fits for a very large range of values of δ [46].

In this paper we approach the problem of understanding general properties of the Voronoi tessellations by joining on the two extreme situations of perfectly deterministic, regular tessellation, to the tessellation resulting from a set of points X generated with a Poisson point process.

We first consider three regular polygonal tessellations of the plane, the honeycomb hexagonal, the square, and triangular tessellations. They are obtained by setting the points x_i as vertices of regular triangles, squares, and hexagons, respectively. Hexagonal tessellation has such peculiar properties of robustness relies on the fact that it is optimal both in terms of perimeter-to-area ratio and in terms of *cost* [50, 51]. The *extremal* properties of such a tessellation are clearly highlighted by [52], where it is noted that a Gibbs system of repulsive charges in 2D arranges spontaneously for low temperatures (freezes) as a regular hexagonal crystal. Moreover, a regular hexagonal structure has been found for the Voronoi tessellation built from the spontaneously arranged lattice of hot spots (strongest upward motion of hot fluid) of the Rayleigh-Bènard convective cells, with the compensating downward motion of cooled fluid concentrated on the sides of the Voronoi cells [23]. This is related to the fact that, under specific parameters ranges, the stationary solutions of the 2D Swift-Hohemberg equation generate naturally hexagonal tessellations [53].

Moreover, we analyze three cubic crystals covering the 3D Euclidean space, namely the simple cubic (SC), the face-centered cubic (FCC) and the body-centered cubic (BCC) lattices [15]. The corresponding space-filling Voronoi cells of such crystals are the cube, the rhombic dodecahedron, and the truncated octahedron. The cubic crystal system is one of the most common crystal systems found in elemental metals, and naturally occurring crystals and minerals. These crystals feature truly extraordinary geometrical properties. The cube is the only space-filling regular solid. The FCC (together with the Hexagonal Close Packed structure) features the largest possible packing fraction: the related 1611 Kepler's conjecture has been recently proved by [54] The Voronoi cell of BCC has been conjectured by Kelvin in 1887 as being the space-filling cell with the smallest surface to volume ratio, and only recently two counter-examples have been given in [55] and [56]. Interestingly, Gabbrielli [56] found a novel space-filling cell by imaginatively looking at the patterns generated as stationary solution of the 3D Swift-Hohenberg equation, thus methodologically mimicking the more usual 2D case. Finally, the truncated octahedron is conjectured to have the lowest *cost* among all 3D space-filling cells [51]. These mathematical properties correspond to very important physical features. Because of its low density, basically due to the low packing faction, the SC system has a high energy structure and is rare in nature, and it is found only in the alpha-form of Po. The BCC is a more compact system and have a low energy structure, is therefore more common in nature. Examples of BCC structures include Fe, Cr, W, and Nb. Finally, thanks to its extremal properties in terms of packing fraction and the resulting high density, FCC crystals are fairly common and specific examples include Pb, Al, Cu, Au and Ag.

The extremal properties in terms of surface–to-area ratio of the hexagonal (in 2D) and truncated octahedral (in 3D) tessellations imply that they may serve as optimal tool for achieving data compression [57]. Another similarity of these two tessellations is related to their topologically stability with respect to infinitesimal perturbations to the position of the lattice points [58].

Using an ensemble-based approach, we study the break-up of the symmetry of the 2D and 3D crystals and quantitatively evaluate how the statistical properties of the resulting Voronoi cells change when we perturb the positions of the lattice points x_i, with a spatially homogeneous Gaussian noise of param

In the 2D case, we analyze *n*, *P*, and *A*, corresponding to the number of sides, the perimeter and the area of each Voronoi cell, respectively. In the 3D case, we focus our interest on *f*, *A*, and *V*, corresponding to the number of faces, the surface area and the volume of each Voronoi cell, respectively.

2.b. Some Exact Results

2.b.1. 2D Tessellations

If we consider a regular square grid of points x_i with sides $l = |v_1| = |v_2|, v_1 \perp v_2$, the Voronoi cell Π_i corresponding to x_i is given by the square centered in x_i with the same side length and orientation as the x_i grid, so that the grid of the vertices y_i of the tessellation is translated with respect to the x_i grid by $l/2$ in both orthogonal directions (the verse is not relevant). Therefore, the vertices of the Voronoi tessellation resulting from the points y_i are nothing but the initial points x_i. If l l $_0^{1/2}$ $|v_1|$ $|v_2|$

variance $\left|\varepsilon^2\right|$. We define $\left|\varepsilon^2\right| = \alpha^2 l_S^2$, thus expressing the mean squared displacement as a fraction α^2 of the natural squared length scale, where $l_S^2 = \rho_0^{-1}$ in the 2D case and $l_S^2 = \rho_0^{-2/3}$ in the 3D case. When ensembles are considered, the probability distribution of the points x_i is still periodic. The parameter can be loosely interpreted as a normalized temperature of the lattice. By def

have consistently verified that when choosing any tolerance smaller than $\xi = 10^{-8}$ we obtain basically the same results.

Figure 1. Ensemble mean of the mean - (a) - and of the standard deviation – (b) – of the number of sides (n) of the Voronoi cells. Note that in (a) the number of sides of all cells is 4 (3) - out of scale - for α=0 in the case of regular square (triangular) tessellation. Half-width of the error bars is twice the standard deviation computed over the ensemble. Poisson-Voronoi limit is indicated.

(a)

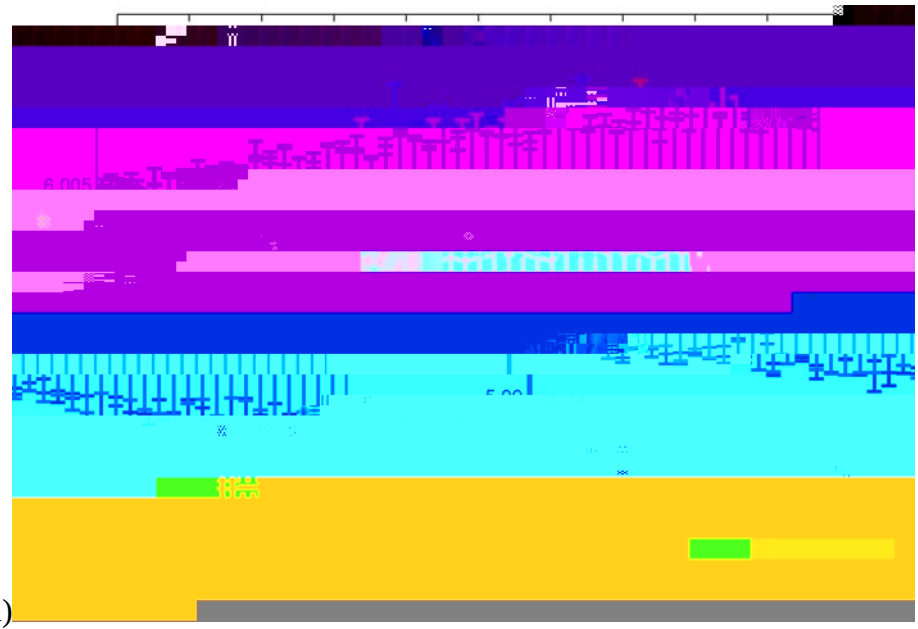

(b)

3. Results

3.a Two-dimensional case

3.a.1 Number of sides of the cells

In the case of the regular square tessellation, the introduction of a minimal amount of symmetry-breaking noise induces a transition in the statistics of $\mu(n)$ and $\sigma(n)$, since $\langle\mu(n)\rangle$ and $\langle\sigma(n)\rangle$ are discontinuous in $\alpha = 0$. In Figs. 1a)-1b) we plot the functions $\langle\mu(n)\rangle$ and $\langle\sigma(n)\rangle$; the half-width of the error bars are twice the corresponding values of $\delta[\mu(n)]$ and $\delta[\sigma(n)]$, whereas the Poisson-Voronoi values are indicated for reference. We have that $\langle\mu(n)|_{\alpha=0}\rangle = 4 \neq 6 = \langle\mu(n)|_{\alpha=0^+}\rangle$, where by $\langle\bullet\rangle|_{\alpha=0+}$ we mean the limit for infinitesimal noise of the quantity $\langle\bullet\rangle$, practically obtained by considering very small positive values of the parameter α. The regular square tessellation results to be structurally

range. Since the presence of a Gaussian noise induces for each point x_i a probability distribution with – an unrealistic- non-compact support, it is possible to

3.a.2 Area and Perimeter of the cells

For all of the perturbed regular tessellations considered in this study, the parametric dependence on α of the statistical properties of the area of the Voronoi cells is more regular than for the case of the number of sides. Results are shown in Figs. 2a)-2b).

In general, the ensemble mean value $\langle \mu(A) \rangle$ of the area of the Voronoi cells is, basically by definition, constrained to be $\rho_0 \langle \mu(A) \rangle = 1$ for all values of α, whereas for all perturbed tessellations the size of fluctuations $\delta[\mu(A)]$ increases with α and reaches for $\alpha > 3$ an asymptotic value, coinciding with that observed in the Poisson-Voronoi case. The α-dependence of $\langle \sigma(A) \rangle$ is more interesting. We first note that the functe that the f

triangular tessellation has a worse agreement with this low-noise approximation. Moreover, for $\alpha > 2$, $\langle\sigma(P)\rangle$ becomes undistinguishable from the asymptotic value realized for Poisson-Voronoi process, given by $\rho_0\langle\sigma(P)|_{PV}\rangle \approx 0.98$.

Figure 3. Ensemble mean of the mean - (a) - and of the standard deviation – (b) – of the perimeter (P) of the Voronoi cells. Half-width of the error bars is twice the standard deviation computed over the ensemble. Poisson-Voronoi limit is indicated. In (b), linear approximation for small values of α is also

The results of the three perturbed regular tessellations basically agree for $\alpha > 0.5$, thus confirming what shown previously. In particular, for $\alpha > 2$, the results coincide with what resulting from the Poisson-Voronoi case. In this regime, we verify the Lewis law [61], *i.e.* $\langle \mu(A) \rangle_n \approx a_1/\rho_0 (n + a_2)$. Our data give $a_1 \approx 0.23$, which is slightly less than what resulting from an asymptotic computation [48], where obtained a linear coefficient of 0.25 is reported. Secondly, and more interestingly, we confirm that Desch's law [62] is violated, *i.e.* $\langle \mu(P) \rangle_n \neq b_1(n + b_2)$, as shown, e.g., in [46]. Nevertheless, instead of a polynomial dependence on *n*, we find that a square root law can be established, i.e. $\langle \mu(P) \rangle_n \approx c_1/\sqrt{\rho_0}\left(\sqrt{n + c_2}\right)$. Our data give $c_1 \approx 1.71$, again slightly less than the asymptotic computation [48], where $c_1 = \sqrt{\pi} \approx 1.77$ is obtained. We note that the Lewis law and such a law allow the establishment of a weakly *n*-dependent relationship such as $\langle \mu(A) \rangle_n \propto \left[\langle \mu(P) \rangle_n\right]^2$, which seems to fit properly with a well-defined 2D isoperimentric ratio $q = 4\pi A/P^2$

corresponds to expressing ( ) 4 ' '. Therefore, if

$$\left(\quad = 0_{+} \right) = 2$$

16, whereas, as shown in [58], the disappearance of the quadrivalent vertices in the rhombic dodecahedron case (FCC crystal) causes an increase of two units (up to exactly 14) in the average number of faces. Near $\alpha = 0$, for both SC and FCC perturbed crystals, $\langle \mu(f) \rangle$ depends linearly on α as $\langle \mu(f) \rangle \approx \langle \mu(f) \rangle\big|_{\alpha=0+} + \gamma\alpha$. The proportionality constant has opposite sign in the two cases, with $\gamma \approx -1.5 \pm 0.05$ for the SC case and $\gamma \approx 1 \pm 0.05$ for the FCC case.

Figure 7. Ensemble mean of the mean and of the standard deviation of the number of faces of the Voronoi cells for perturbed SC, BCC and FCC cubic crystals. The error bars, whose half-width is twice the standard deviation computed over the ensemble, are too small to be plotted. The Poisson-Voronoi limit is indicated.

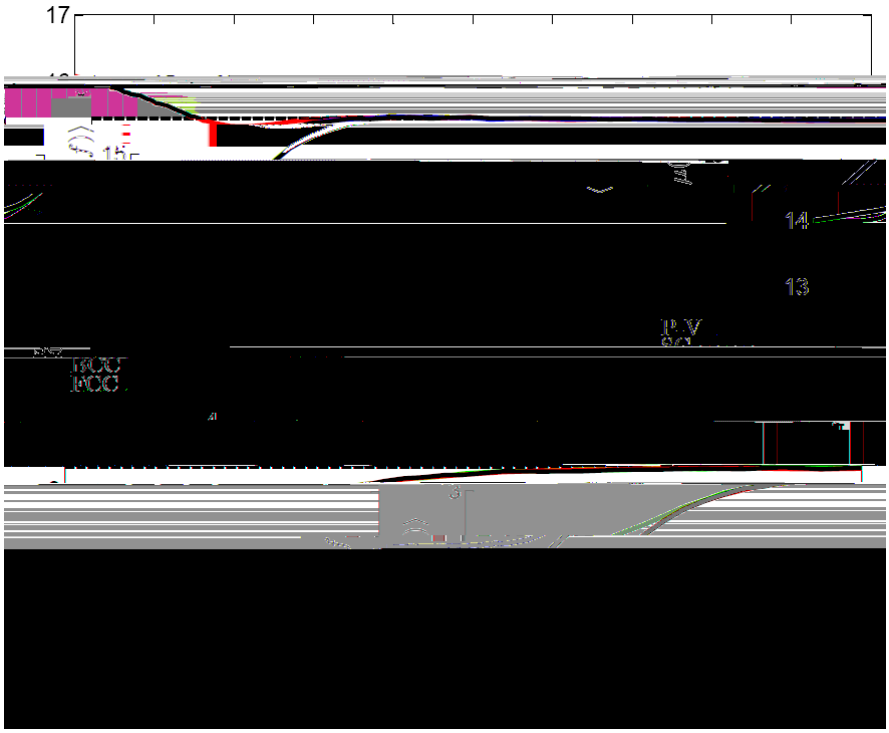

Moreover, the introduction of noise generates the sudden appearance of a finite standard deviation in the number of faces in each cell $\langle \sigma(f) \rangle\big|_{\alpha=0+}$, which is larger fo, whicc656 Q76f6122 Tr th22 6039 Tm(o)T

Figure 8. Ensemble mean of the standard deviation of the volume (V) of the Voronoi cells for perturbed SC, BCC and FCC cubic crystal. The ensemble mean of the mean is set to the inverse of the density. Values are multiplied times the appropriate power of the density in order to obtain universal functions. The error bars, whose half-width is twice the standard deviation computed over the ensemble, are too sm

When considering the area of the

Phelan structure has a smaller surface [55]. It is reasonable to expect that a similar quadratic increase of the average surface should be observed when perturbing with spatial gaussian noise the crystalline structure corresponding to the Weaire-Phelan cell. For $\alpha > 0.3$, the values of

Figure 11. Ensemble m

For $\alpha \geq 0.5$ the results for the SC, FCC and BCC crystals basically agree and converge to the Poisson-Voronoi limit for $\alpha \geq 1$. Therefore, whereas the Voronoi tessellation of the BCC crystal is the most stable against noise when the topological properties of the cells are considered (see Fig. 7), when analyzing the shape of the cells from a metrical point of view, the FCC crystal is actually the most stable.

In order to further clarify the variability of the shapes of the cells, we take advantage of a strategy of investigation commonly adopted for studying Voronoi tessellations, *i.e.* the stratification of the expectation values of the geometrical properties with respect to classes defined by the number of sides of the cells [46, 48, 59]. In the present case, it would be profitable to study quantities such as $\langle \mu(V) \rangle|_f$ and $\langle \mu(A) \rangle|_f$, where the pedix indicates that the averages are performed only on cells with *f* faces. It is readily observed that, in all cases, both $\langle \mu(V) \rangle|_f$ and $\langle \mu(A) \rangle|_f$ increase with *f* (not shown), for the basic and intuitive reason that cells with a larger num

seen, in the considered Voronoi tessellations the cells are definitely not similar, with larger (and more faceted) cells associated to larger isoperimetric quotients. In order to quantify this, we take the following approach. We consider the possibility of a scaling law approximating the (statistical) relationship between the volume and the area of the cells of the form $V(A)=\varepsilon(A)A^{3/2}$ with $\varepsilon(A)=\varepsilon' A^{\eta'}$, so that , if $\eta'>0$, $\varepsilon(A)$ is monotonically increasing with *A*, It should be mentioned that this parameterization of $\varepsilon(A)$ amounts to defining *Q* as ( )

In all cases we find that $\langle\eta\rangle$ is larger than 3/2, with typical uncertainties of the order of at most $2\cdot10^{-3}$. Therefore $\langle\eta'\rangle$ is always larger than zero: such an anomalous scaling implies that, typically, a cell with a larger volume has a relatively smaller surface, and, in other terms, a larger isoperimetric quotient (which increases $\propto A^{2\eta'}$).

Figure 13. Ensemble mean of the scaling exponent η fitting the power-law relation $V \propto A^{\eta}$ for the Voronoi cells of perturbed SC, BCC and FCC cubic crystals. The presence of an anomalous scaling $(\eta > 3/2)$ due to the fluctuations in the shape of the cells is apparent. The error bars, whose half-width is twice the standard deviation computed over the ensemble, are too small to be plotted. The Poisson-Voronoi limit (see Fig. 12) is indicated. Details in the text.

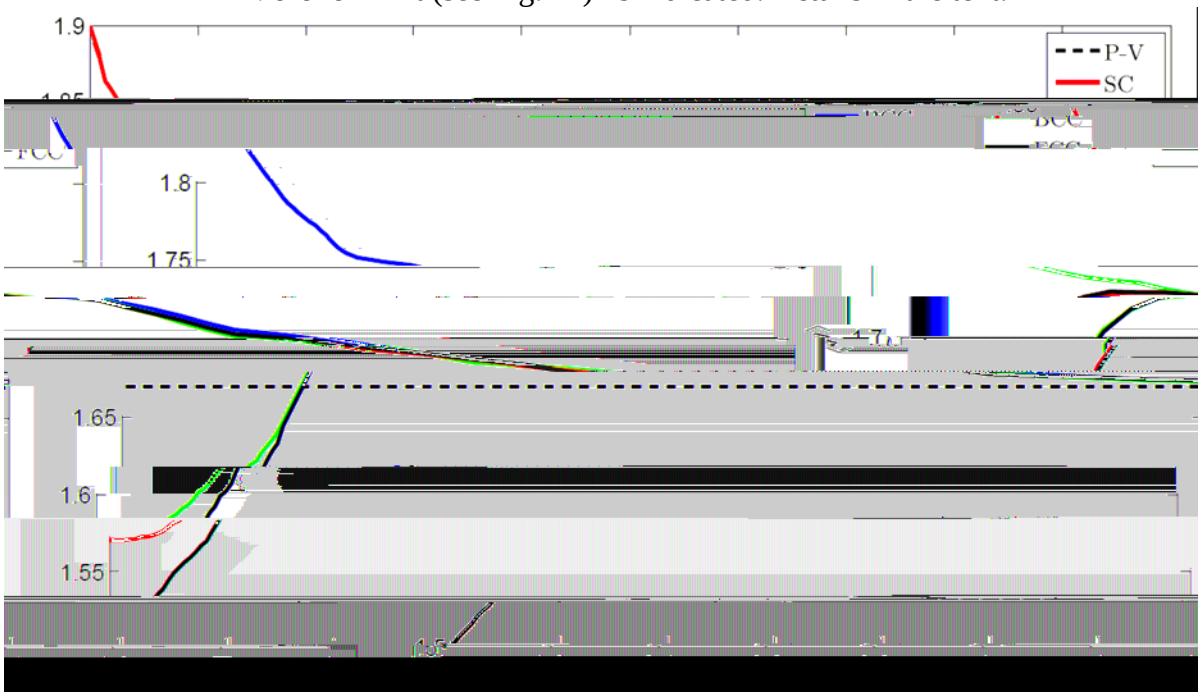

In particular, in the Poisson-Voronoi limit $\eta \approx 1.67$ - black line in Fig. 12 - which suggests the occurrence of a 5/3 exponent. It is also remarkable that, as soon as noise is turned on, anomalous scaling due to is observed in for the SC and BCC cubic crystals. In the SC case, $\eta(\alpha = 0_+) \approx 1.88$, the exponent is monotonically decreasing for all values of α, and becomes undistinguishable from the Poisson-Voronoi limit for $\alpha > 2$. In the BCC case, as opposed to what one could expect given the structural stability of the crystal, ( )

As mentioned before, the number of faces provides a good proxy indicator for the shape of the cell, or, more precisely, of its isoperimetric quotient. In order to find a robu

have that the topology of these tessellations is robust also against small but finite noise. For strong noise, the statistical properties of the tessellations of the perturbed crystals converge to those of the Poisson-Voronoi limit, but, quite notably, the memory of the specific initial unperturbed state is lost already for moderate noise, since the statistical properties of the perturbed tessellations are typically indistinguishable for $\alpha > 0.5$.

In the case of perturbed square (triangular) tessellation, for a specific intensity of the noise determined by $\alpha = \alpha_m \approx 0.25$ ($\alpha = \alpha_m \approx 0.5$), it is possible to minimize the mean isoperimetric ratio of the Voronoi cells, whereas by choosing $\alpha = \alpha_M \approx 0.75$ we obtain a relative maximum for perime

Symmetry **2009**,

References

1. Voronoi G. (1907). Nouvelles applications des paramètres continus à la théorie des formes quadratiques. Premier Mémoire: Sur quelques propriétées des formes quadritiques positives parfaites. J. Reine Angew. Math. 133:97-178.
2. Voronoi G. (1908). Nouvelles Applications des Parametres Continus a la Theorie des Formes Quadratiques. Duesieme Memoire: Recherches sur les Parallelodères Primitifs, J. Reine Angew. Math. 134:198-287.
3. Isokawa Y., (2000). Poisson-Voronoi tessellations in three-dimensional hyperbolic spaces, Adv. Appl. Probl. 32, 648-662.
4. Okabe, A., Boots B., Sugihara K., and Chiu S. N. Spatial Tessellations - Concepts and Applications of Voronoi Diagrams. 2nd edition. Wiley, London, 2000.
5. Sortais M., Hermann S., and Wolisz A. (2007). Analytical Investigation of Intersection-Based Range-Free Localization Information Gain. In: Proc. of European Wireless 2007.
6. Finney, J. L. (1975). Volume occupation, environment and. accessibility in proteins. The problem of the protein surface. J. Mol. Biol. 96, 721–732.
7. Icke V (1996). Particles, space and time, Astrophys. Space Sci., 244, 293-312.
8. Barrett T. M. (1997). Voronoi tessellation methods to delineate harvest units for spatial forest planning, Can. J. For. Res. 27(6): 903–910.
9. Goede A., Preissner R., and Frömmel C. (1997). Voronoi cell: New method for allocation of space among atoms: Elimination of avoidable errors in calculation of atomic volume and density, J. of Comp. Chem. 18 1113-1118.
10. Weaire D., Kermode J.P., and Wejchert J. (1986). On the distribution of cell areas in a Voronoi network. Phil. Mag. B, 53, L101–L105.
11. Dotera T. (1999). Cell Crystals: Kelvin's Polyhedra in Block Copolymer Melts, Phys. Rev. Lett. 82, 105–108.
12. Bennett, L. H., Kuriyama, M., Long, G. G., Melamud, M., Watson, R. E., and Weinert, M. (1986). Local atomic environments in periodic and aperiodic Al-Mn alloys, Phys. Rev. B 34, 8270-8272.
13. Li S., and Wongsto A. (2004). Unit973.60028sTuJz8d582-O Td[J. Molelv4R738 -echanTw 22a2411ses

60. Lucarini V. (2009), Three-Dimensional Random Voronoi Tessellations: From Cubic Crystal Lattices to Poisson Point Processes, J. Stat. Phys . 134, 185-206
61. Lewis F. T., (1928). The correlation between cell division and the shapes and sizes of prismatic cells in the epidermis of Cucumis, Anat. Rec., 38. 341-376.
62. Desch C. H. (1919). The solidification of metals from the liquid state, J. Inst. Metals, 22, 241.
63. Finch S. R., Mathematical Constants, Cambridge University Press, Cambridge, 2003.
64. Geim, A. K., and K. S. Novoselov, The rise of graphene, *Nature Materials* **6**, 183 - 191 (2007) doi:10.1038/nmat1849
65. Hilhorst H. J. (2009). Heuristic theory for many-faced d-dimensional Poisson-Voronoi cells, arXiv:cond-mat/0906.4449v1
66. Dodson C. T. J. (2008), On the entropy flows to disorder, arXiv:math-ph /0811.4318v2
67. Coles, S. G., An Introduction to Statistical Modeling of Extreme Values, Springer, London, 2001

© 2009 by the authors; licensee Molecular Diversity Preservation International, Basel, Switzerland. This article is an open-access article distributed under the terms and conditions of the Creative Commons Attribution license (http://creativecommons.org/licenses/by/3.0/).